Author(s): de Groote, R. P.; Nesterenko, D. A.; Kankainen, A.; Bissell, M.L.; Beliuskina, O.; Bonnard, J.; Campbell, P.; Canete, L.; Cheal, B.; Delafosse, C.; de Roubin, A.; Devlin, C.S.; Dobaczewski, J.; Eronen, T.; Garcia, Ruiz R. F.; Geldhof, S.; Gins, W.; Hukkanen, M.; Imgram, P.; Mathieson, R.; Koszorús, Á.; Moore, I.D.; Pohjalainen, I.; Reponen, M.; van den Borne, B.; Vilén, M.; Zadvornaya, S.

Title: Measurements of binding energies and electromagnetic moments of silver isotopes : A complementary benchmark of density functional theory

Year: 2024

Version: Published version

Phys. Lett. B 848 (2024) 138352

Contents lists available at ScienceDirect

Physics Letters B

journal homepage: www.elsevier.com/locate/physletb

Letter

Measurements of binding energies and electromagnetic moments of silver isotopes – A complementary benchmark of density functional theory

R.P. de Groote [a,b,*], D.A. Nesterenko [a], A. Kankainen [a], M.L. Bissell [c], O. Beliuskina [a], J. Bonnard [d,e], P. Campbell [c], L. Canete [a], B. Cheal [f], C. Delafosse [a], A. de Roubin [a], C.S. Devlin [f], J. Dobaczewski [d,g], T. Eronen [a], R.F. Garcia Ruiz [h,i], S. Geldhof [a], W. Gins [a], M. Hukkanen [a,j], P. Imgram [k], R. Mathieson [f], Á. Koszorús [f], I.D. Moore [a], I. Pohjalainen [a], M. Reponen [a], B. van den Borne [b], M. Vilén [a], S. Zadvornaya [a]

[a] Accelerator Laboratory, Department of Physics, University of Jyväskylä, PB 35(YFL) FIN-40351 Jyväskylä, Finland
[b] KU Leuven, Instituut voor Kern-en Stralingsfysica, B-3001 Leuven, Belgium
[c] Department of Physics and Astronomy, University of Manchester, Manchester M13 9PL, United Kingdom
[d] Department of Physics, University of York, Heslington, York YO10 5DD, United Kingdom
[e] Université de Lyon, Institut de Physique des 2 Infinis de Lyon, IN2P3-CNRS-UCBL, 4 rue Enrico Fermi, 69622 Villeurbanne, France
[f] Department of Physics, University of Liverpool, Liverpool L69 7ZE, United Kingdom
[g] Institute of Theoretical Physics, Faculty of Physics, University of Warsaw, ul. Pasteura 5, PL-02-093 Warsaw, Poland
[h] CERN, CH-1211 Geneva 23, Switzerland
[i] Massachusetts Institute of Technology, Cambridge, MA 02139, USA
[j] Université de Bordeaux, CNRS, LP2I Bordeaux, UMR 5797, F-33170 Gradignan, France
[k] Institut für Kernphysik, Technische Universität Darmstadt, D-64289 Darmstadt, Germany

ARTICLE INFO

Editor: B. Blank

ABSTRACT

We report on a set of high-precision measurements of nuclear binding and excitation energies, as well as nuclear spins, magnetic dipole and electric quadrupole moments of neutron-rich silver isotopes, $^{113-123}$Ag. The measurements were performed using the JYFLTRAP mass spectrometer and the collinear laser spectroscopy beamline at the Ion Guide Isotope Separator On-Line (IGISOL) facility. For the first time, we can firmly establish the ordering of the long-lived $I^{\pi} = 1/2^{-}$, $7/2^{+}$ states in these isotopes, and pin down the inversion of these two levels at either $A = 121$ ($N = 74$) or $A = 123$ ($N = 76$). We compare these findings to calculations performed with density functional theory (DFT), from which we establish the crucial role that the spin-orbit strength and time-odd mean fields play in the simultaneous description of electromagnetic moments and nuclear binding.

1. Introduction

Understanding the structure of atomic nuclei, and its evolution as the number of nucleons changes, requires a comprehensive study of different nuclear properties and continuous development of predictive nuclear methods [1]. Electromagnetic moments and binding energies provide essential information on the validity of theoretical advances, and serve to stringently test predictions through their sensitivity to collectivity and valence nucleon configurations [2–9]. *Ab-initio* approaches and nuclear density functional theory (DFT) have been shown to provide an emerging microscopic understanding of nuclear structure [10–15]. The fruitful dialogue between experiment and theory was recently highlighted through measurements of the magnetic moments of indium ($Z = 49$), which challenged the single-particle interpretation of their structure [16]. In this letter, we further test DFT calculations, by moving towards a more complicated open-shell system and by comparing simultaneously to measurements of masses, excitation energies, spins, magnetic dipole and electric quadrupole moments of silver isotopes ($Z = 47$). The measurements span between mass numbers $A = 113 - 123$; the mean-squared charge radii were already published [17]. We perform DFT calculations, which self-consistently take into account core-polarization effects, essential for the description of nuclear moments, and thus allow for the use of bare single-particle charges and g-factors [14,15]. In doing so, we demonstrate an ability to predict all

* Corresponding author.
E-mail address: ruben.degroote@kuleuven.be (R.P. de Groote).

https://doi.org/10.1016/j.physletb.2023.138352
Received 3 May 2023; Received in revised form 6 October 2023; Accepted 20 November 2023
Available online 24 November 2023

measured observables, and the complementary sensitivity of the observables to different aspects of the nuclear functionals.

Due to the proximity of low-j ($2p_{1/2}$) and high-j ($1g_{9/2}$) proton orbitals, isomerism ($t_{1/2} >$ ms) is common in the silver isotopes. The spin of the ground state has not yet been firmly established along the chain, though it is known that the $1/2^-$ state is isomeric in ^{99,101,103}Ag, and becomes the ground state at $A = 105$. The ground state in ^{97,99,101}Ag has a spin–parity of $9/2^+$, as is predicted also for ^{125,127}Ag. For the mid-shell odd-A isotopes $^{103-123}$Ag, a $7/2^+$ state becomes the second long-lived state in addition to the $1/2^-$ state. Above $A = 119$, it is not known which state is the ground state and which is the isomer. Recently, a $1/2^-$ beta-decaying isomer in ^{123}Ag was identified based on gamma-ray transitions to the $1/2^-$, $9/2^+$ and $7/2^+$ states [18], indicating a re-inversion of the $1/2^-$ and $7/2^+$ states occurs at some point in the chain. In this work, combined with the first detailed laser spectroscopy study on neutron-rich silver isotopes, we can unambiguously establish both the spin-parities and the ordering of the studied states using the phase-imaging ion cyclotron resonance technique [19].

2. Experimental procedure

Radioactive silver isotopes were produced at the IGISOL facility in the Accelerator Laboratory of the University of Jyväskylä, using proton-induced fission on a thin uranium foil. The fission products were stopped and thermalized in a helium-filled gas cell operated at a pressure of 300 mbar, and extracted using a sextupole ion guide [20]. The majority of the extracted products were singly-charged ions. After accelerating to 30 kV, the ions were mass-separated using a 55° dipole magnet, injected into a radiofrequency quadrupole RFQ [21], where they were cooled and bunched. The ion bunches were delivered either into the JYFLTRAP double Penning trap [22], or to the collinear laser spectroscopy beamline [23,24].

2.1. Collinear laser spectroscopy

Collinear laser spectroscopy was performed after a 100 ms cooling and bunching time, using the same methodology as presented in [25]. The ions were neutralized via charge-exchange processes using a charge-exchange cell (CEC) filled with hot potassium vapour. By applying an acceleration potential to the cell, the atoms could be Doppler-shifted into resonance with the counter-propagating laser beam. Spectroscopy was performed from the $4d^{10}5s\ ^2S_{1/2}$ atomic ground state to the $4d^{10}5p\ ^2P_{3/2}$ state, by detecting the fluorescence emitted at 328.1624 nm. For the first experimental run, the laser light was produced using an intra-cavity doubled Spectra Physics 380 dye laser, pumped by a 5 W Verdi 532 nm laser. The following two experimental runs instead used a Matisse DS dye laser pumped by a 10 W Millenia 532 nm laser, frequency doubled using a Matisse WaveTrain. In all campaigns, the dye laser was frequency stabilized to a HighFinesse WSU-10 wavelength meter. Given the large hyperfine splittings of the $I = 7/2^+$ states, the laser wavelength was chosen to keep the Doppler-tuning voltage between 0 and 2 kV. Hyperfine structures were thus obtained by recording the number of photon counts observed by a Photo-Multiplier Tube as function of the wavelength in the rest frame of the atoms.

Regular reference measurements were performed on ^{109}Ag using beams from an offline ion source [26] to detect possible drifts in wavemeter calibration or the ion beam energy. For all odd-A silver isotopes, two states could be observed in the hyperfine spectra (see Fig. 1). The analysis was performed using the SATLAS package [27]. By taking the magnetic dipole A and electric quadrupole B constants in ratio with the moments of ^{109}Ag, the magnetic dipole (μ) and electric quadrupole (Q) moments of the isotopes of interest can be extracted. We used the references suggested in [28,29]: $\mu_{109} = -0.1306906(2)\,\mu_N$ (obtained by correcting experimental data [30] for diamagnetism [31]), $A_{S_{1/2},109} = -1976.932075(17)$ MHz [32], $Q_{110m} = +1.44(10)$ b [33] and $B_{P_{3/2},110m} = 425(18)$ MHz [34]. For the determination of the magnetic dipole moment we opted to neglect the hyperfine anomaly, which might be as large as a few percent [5], but will require further work to evaluate. For the spin-$1/2^-$ states, the upper-state splitting cannot be resolved. We thus fixed the ratio of hyperfine A constants to the literature ratio of 53.4, determined using the average of two upper-state A-constants available in literature ($A_{P_{3/2},109} = -36.7(7)$ [35] and $A_{P_{3/2},109} = -37.3(8)$ [36]).

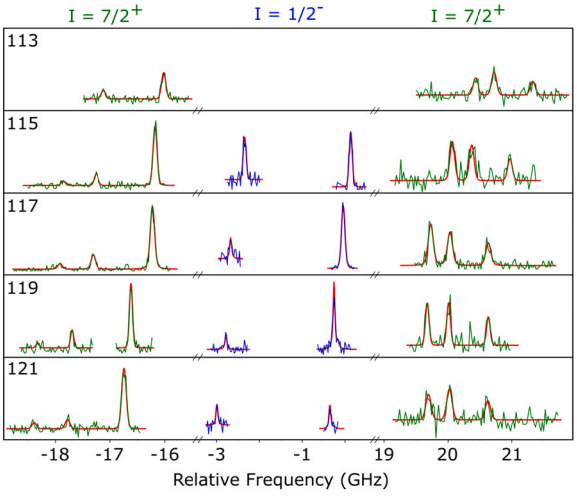

Fig. 1. Example hyperfine spectra of the radioactive odd-A silver isotopes. For the $I = 1/2^-$ state (middle two peaks), the left peak near -3000 MHz is considerably smaller than the right peak; more time was spent gathering statistics on those channels, by a factor of 2 or 3 depending on the isotope. The vertical scale was furthermore increased to make the resonances more clearly visible.

2.2. Penning-trap mass spectrometry

The mass measurements on singly-charged ions were performed using the PI-ICR technique [19,37] at the JYFLTRAP double Penning trap [22]. More details can be found in [38]. The ions were cooled, purified and centred using the mass-selective buffer-gas cooling technique [39] in the first trap and transferred to the second trap. After a few ms, the purified ions of interest were transferred back to the preparation trap for additional cooling. Finally, the ions of interest with charge-to-mass ratio q/m were sent to the measurement trap, where their cyclotron frequency $\nu_c = qB/(2\pi m)$ in the magnetic field B was determined.

The phase-accumulation time in the PI-ICR method was chosen to separate the isomeric states of the silver isotopes, while ensuring no overlap with possible contamination. The phase-accumulation time was about 800 ms for ^{113}Ag, 1 s for ^{115}Ag, 1.3 s for ^{117}Ag, 1.2 s for ^{119}Ag, 600 and 700 ms for ^{121}Ag and 400 ms for ^{123}Ag. An example of the phase spots seen on the position-sensitive detector for ^{123}Ag is highlighted in Fig. 2. The atomic masses were determined as $M = \frac{\nu^{c,ref}}{\nu_c}(M_{ref} - m_e) + m_e$, where m_e is the electron mass, $\nu^{c,ref}$ and M_{ref} are the measured cyclotron frequency and atomic mass [40] for the reference. The systematic uncertainties were included in the final uncertainty of the cyclotron frequency ratios [41]. The count-rate class analysis [42] was performed for the frequency ratios to take into account ion-ion interactions.

3. Results and discussion

Our results are summarized in Table 1. Fig. 3(a) shows the energy difference between the $1/2^-$ and $7/2^+$ states. Two long-lived states were measured separately for the first time for all isotopes, except ^{121}Ag. For ^{121}Ag, a small number of ions 250.6(36) keV above the long-lived state were observed but the energy is not in line with the trend of other isomeric states. Most likely, the ions are ^{105}Nb^{16}O$^+$, which is closest to the observed value based on the SCM_Qt program [43]. Due to the

Table 1
Summary of the spin-parity I^π, hyperfine constants A and B, dipole moment μ, quadrupole moment Q, reference ion for the mass and excitation energy measurements, frequency ratios ν_c^{ref}/ν_c, mass-excess values $\Delta = (M - A)c^2$ and excitation energies E_x. For Q, the error indicates the combination of the statistical uncertainty and the uncertainty on B/Q. See text for discussion on the spin assignments.

Nuclide	I^π	$A(S_{1/2})$ [MHz]	$\mu[\mu_N]$	$B(P_{3/2})$ [MHz]	Q [b]	Ref.	ν_c^{ref}/ν_c^{int}	Δ (keV)	E_x (keV)
^{107}Ag	$1/2^-$	-1712(3)	-0.1132(2)	–	–				
^{109}Ag	$1/2^-$	-1978(1)	-0.13074(3)	–	–				
^{113}Ag	$1/2^-$	–	–	–	–	^{113}Ag^m	0.999 999 564(37)	-86964.0(51)	–
^{113}Ag^m	$7/2^+$	+9609(5)	+4.447(2)	+305(12)	+1.03(9)	^{133}Cs	0.849 525 774(27)	-86918.1(34)	45.8(39)
^{115}Ag	$1/2^-$	-2577(13)	-0.1704(9)	–	–	^{115}Ag^m	0.999 999 658(13)	-84944.9(28)	–
^{115}Ag^m	$7/2^+$	+9556(2)	+4.4223(9)	+309(6)	+1.04(8)	^{133}Cs	0.864 590 363(20)	-84908.3(24)	36.6(14)
^{117}Ag	$1/2^-$	-2651(12)	-0.1752(8)	–	–	^{117}Ag^m	0.999 999 726(28)	-82188.4(37)	–
^{117}Ag^m	$7/2^+$	+9486(2)	+4.3897(8)	+309(5)	+1.05(8)	^{133}Cs	0.879 660 927(17)	-82158.6(22)	29.8(31)
^{119}Ag	$1/2^-$	-2582(14)	-0.1707(9)	–	–	^{119}Ag^m	0.999 999 706(69)	-78648.9(84)	–
^{119}Ag^m	$7/2^+$	+9581(2)	+4.434(1)	+276(7)	+0.93(8)	^{133}Cs	0.894 737 894(28)	-78616.3(35)	32.6(76)
^{121}Ag	$7/2^+$	+9610(3)	+4.447(1)	+249(10)	+0.85(8)	^{133}Cs	0.909 820 3532(91)	-74394.0(11)	–
^{121}Ag^m	$1/2^-$	-2718(7)	-0.1797(4)	–	–	–	(*)		
^{123}Ag	$7/2^+$					^{133}Cs	0.924 907 400(29)	-69603.9(36)	–
^{123}Ag^m	$1/2^-$					^{123}Ag	1.000 000 499(77)	-69546.7(95)	57.2(88)

(*) Only one state was observed for ^{121}Ag in the PI-ICR measurement, as discussed in the main text.

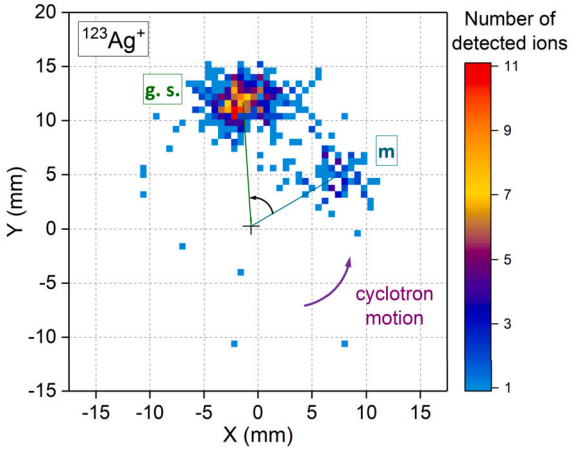

Fig. 2. Projection of the cyclotron motion of $^{123}Ag^+$ ions onto the detector obtained with the PI-ICR technique, using 400 ms phase accumulation time. The coloured bar indicates the number of detected ions in each pixel.

estimated short half-life ($T_{1/2} \approx 200$ ms [44]) and the lower production rate of the $1/2^-$ state in ^{121}Ag, established by the laser spectroscopy, the number of $1/2^-$ ions has to be very low after a measurement cycle of one second in the trap. The single state observed in ^{121}Ag in the PI-ICR measurement was therefore attributed to the more abundant longer-lived $7/2^+$ state ($T_{1/2} = 770(10)$ ms [44]).

Using the relative production ratios of the ground- to isomeric state extracted from the laser spectroscopy data, we can unambiguously assign the measured masses to a specific nuclear state. The excitation energies for ^{113,117}Ag agree well with the literature [45,46] and the mass value of ^{113}Ag with the recently reported value from the Canadian Penning trap [47]. A discrepancy of -4.6(14) keV at ^{115}Ag [48] is observed, which could be explained by low statistics for the ground state and ions detected between the ground and isomeric states in the PI-ICR image spots, potentially caused by a contaminant ion. For ^{119}Ag, we confirm the excitation energy of the $7/2^+$ isomer, and establish the $1/2^-$ state as the ground state in ^{119}Ag. This supports the assignment made in recent decay spectroscopy work on ^{119}Ag [49]. We also confirm the spectroscopy result for the excitation energy of the $1/2^-$ isomer in ^{123}Ag [18]. Therefore, the crossing of the $1/2^-$ and $7/2^+$ states can now be pinpointed to occur at either $A = 121$ or $A = 123$.

For the high-spin state, the analysis of the laser spectroscopy data was performed assuming $I = 5/2^+, 7/2^+, 9/2^+$, from which it was found that only $I = 7/2^+$ yields g-factors in line with the well-established values in the neighbouring indium and rhodium chains. Indeed, for all isotopes of indium, $g \sim 1.23$ (except at $N = 82$ [16]) and for rhodium $g \sim 1.26$. For the new data on the silver isotopes, when fitting with $I = 5/2$ we find $g \sim 1.68$, with $I = 5/2$ we find $g \sim 1.27$, and with $I = 9/2$ we find $g \sim 1$. In the case of ^{113,115,117}Ag, there are also E3 internal transitions reported in [46] which support this conclusion.

The g-factors ($g = \mu/I$) are shown graphically in Fig. 3.(b-c) alongside literature values [50,51,30,52,5]. The g-factors of the $7/2^+$ states are nearly constant throughout the isotopic chain, whereas those of the $9/2^+$ states show an increase towards the single-particle estimate, although it is not reached even at $N = 50$. The g-factors of the $1/2^-$ states exhibit a different trend: a linear decrease until $N = 68$, after which a rather constant value is obtained ($g \approx -0.35$). Similar observations have been made in the indium ($Z = 49$) isotopes [53,16], but there the high-spin state is $9/2^+$ and remains the ground state throughout the chain.

3.1. Comparison to nuclear DFT calculations

We compare these measured experimental observables with DFT calculations, plotted alongside the experimental data in Fig. 3. We performed calculations for $^{97-129}$Ag ($N = 50 - 82$) using code HFODD (v3.16m) [54,55], following the recently developed nuclear-DFT description of nuclear moments [14,16,15]. We determined dipole and quadrupole moments of silver isotopes by analysing three-hole unpaired proton configurations along with paired neutron open-shell configurations and unpaired neutron configurations for the closed-shell $N = 50$ & 82 isotopes. For protons, we occupied prolate-deformed single-particle states with angular momenta Ω aligned along the axial-symmetry axis up to $Z = 50$ and created three types of three-hole configurations: (i) 7/2 configuration – holes in the $[404]_{\pm 9/2}$ and $[413]_{-7/2}$ deformed Nilsson states, (ii) 9/2 configuration – holes in $[413]_{\pm 7/2}$ and $[404]_{-9/2}$, and (iii) 1/2 configuration – holes in $[404]_{\pm 9/2}$ and $[301]_{-1/2}$.

Rotational symmetry was restored by employing the standard angular-momentum projection (AMP) method [56] and the spectroscopic moments were determined for the AMP states.[1] Apart from the lowest angular-momentum states with $I = 7/2^+, 9/2^+$ and $1/2^-$, projected from configurations 7/2, 9/2 and 1/2, respectively, we also considered the $9/2^+$ state projected from the 7/2 configuration, which we denote $I = 9/2(7/2)$. Two different Skyrme functionals were used: the UNEDF1 [57], and a modified version of this functional called

[1] We note that the single-particle observables, such as the nuclear moments studied in this work, are not affected by the singularities of the off-diagonal matrix elements that impact the determination of the symmetry-restored energies [56].

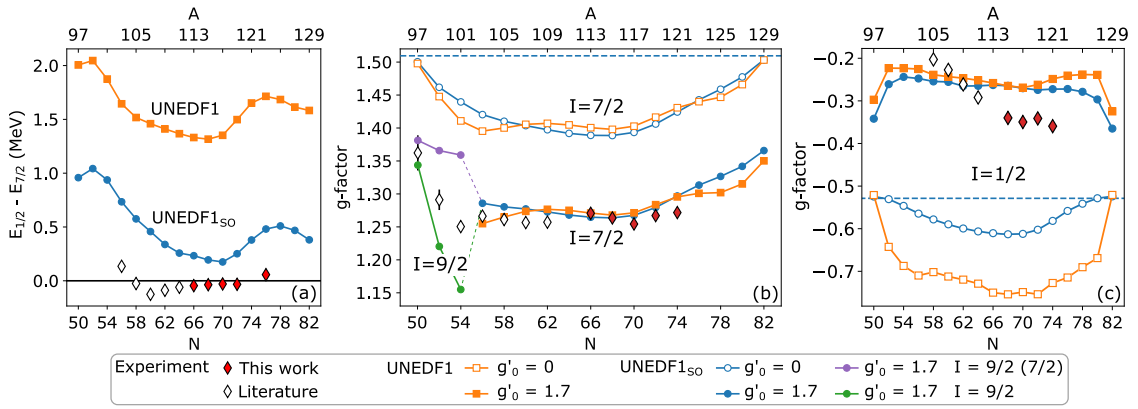

Fig. 3. Experimental results compared to DFT calculations. Panel (a) shows the differences of intrinsic energies between the lowest-lying $I = 1/2$ and $I = 7/2$ states. Panels (b) and (c) show the g-factors ($g = \mu/I$) of the (i) long-lived 9/2 states for $A \leq 101$, (ii) 7/2 states for $A \geq 103$, and (iii) 1/2 states. Diamonds show experimental results. Open (full) symbols show DFT results obtained without (with) time-odd mean fields generated by the spin-spin interaction included. Furthermore, squares (circles) indicate calculations performed with the UNEDF1 (UNEDF1$_{SO}$) functional. The dashed lines show the single-particle (Schmidt) limits.

UNEDF1$_{SO}$ [58] with a higher spin-orbit strength adjusted to the deformed shell structure in the actinides. To show the essential impact of the non-zero core spin distribution on the magnetic moments, we performed calculations with and without the time-odd mean fields generated by the spin-spin interaction. The latter was modelled by the isovector Landau parameter $g_0' = 1.7$ specified according to the methods in Ref. [14,59].

The UNEDF1 functional places the $I = 1/2^-$ state at an excitation energy of about 1.5 MeV, in stark disagreement with the experimental data. The UNEDF1$_{SO}$ functional yields smaller excitation energies, clarifying this discrepancy, suggesting that the spin-orbit strength of UNEDF1 should be globally readjusted using the result obtained in this Letter as an important anchor point. The measured excitation energies may therefore serve as a benchmark for future developments of functionals. Aside from this offset between the two theoretical curves, very similar trends are obtained for both calculations, which agree reasonably well with the experimental trends. Future experimental efforts to measure the energy differences towards $N = 82$ would allow for the apparent turnover in the calculated trend after ^{125}Ag to be probed.

When the time-odd mean fields generated by the spin-spin interaction are *not* included (open circles or squares in Fig. 3), the g-factors land near the single-particle estimates at the neutron shell closures, and gradually drop towards the mid-shell. This drop can be attributed to the coupling between spin and charge distributions; the latter being reflected in the non-zero quadrupole deformations depicted in Fig. 4. Experimentally, significantly smaller magnetic moments are obtained. This difference is considerably larger than a possible effect due to the neglected hyperfine anomaly. By including the time-odd mean fields represented by the Landau parameter g_0', the calculated magnetic moments are brought into agreement with data. Note that the calculations shown in Fig. 3(b) were performed with the value of $g_0' = 1.7(4)$ recommended for the UNEDF1 functional following the global analysis of magnetic moments across the nuclear landscape [14]. This choice of g_0' does not represent a local fit to best match with the data obtained here. The success of DFT calculations in reproducing magnetic moments globally represents a major step forward.

The structure of the $9/2^+$ states appears to be more complex than for $I = 7/2^+$. The g-factors suggest that for all but the semi-magic nucleus ^{97}Ag, the wave function might be a mixture of the $I = 9/2(7/2)$ rotational band member of the 7/2 configuration and the lowest rotational member $I = 9/2^+$ of the 9/2 configuration. Multi-reference codes need to be developed and applied to prove this statement more quantitatively. Along a similar line, it appears that while the approximate size of the g-factors of the $I = 1/2^-$ isotopes can be predicted through the inclusion of time-odd mean fields, this is not sufficient to reproduce the trend observed in experiment.

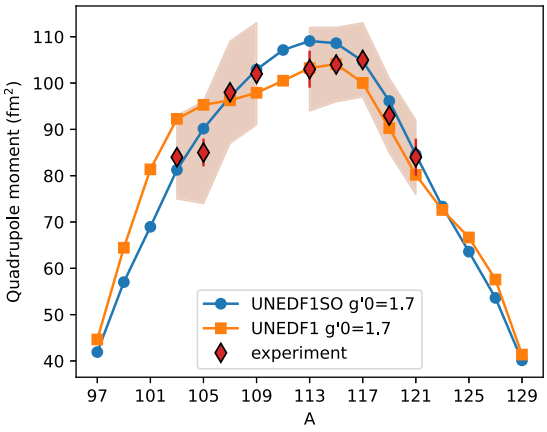

Fig. 4. Comparison of experimental and theoretical spectroscopic quadrupole moments of the $7/2^+$ states. Colour code is the same as in Fig. 3. The red shaded area indicates the uncertainty due the reference B/Q, while the error bars indicate only our statistical uncertainty on B.

Finally, we turn the discussion to the experimental quadrupole moments, plotted in Fig. 4. Alongside statistical error bars determined by experimental aspects, a shaded uncertainty band is also shown, due to the uncertainty of the electric field gradient (V_{zz}) used to determine the quadrupole moment of the reference isotope (^{110}Ag). A revised value of V_{zz} would merely shift all data uniformly up or down within the indicated area. The quadrupole moment is not sensitive to the time-odd mean fields, much like the excitation energies, but does display some sensitivity to the choice of spin-orbit strength, as shown in Fig. 4. The UNEDF1 functional produces a trend with a flatter top as compared to UNEDF1$_{SO}$, which instead yields a more parabolic trend.

4. Conclusions and outlook

In conclusion, we reported on measurements of magnetic dipole and electric quadrupole moments, nuclear spins, binding and excitation energies of $^{113-123}$Ag. We firmly established the ordering of the long-lived $I^\pi = 1/2^-,\ 7/2^+$ states and showed that the inversion of these two levels occurs at $A = 121$ ($N = 74$) or $A = 123$ ($N = 76$). Comparing with DFT calculations, several conclusions are drawn. Firstly, the energy difference of the $I = 1/2^-, 7/2^+$ states is very sensitive to the strength of spin-orbit terms. Secondly, the DFT calculations reproduce the magnitude of dipole and quadrupole moments without the need for localized effective factors, proving its suitability for a global description of these observables. This work also highlights the importance of

measuring complementary observables. Indeed, in this case the most sensitive way to characterise the spin-orbit strength entering DFT calculations is primarily through the mass measurements, while the time-odd mean fields are best constrained through the study of the magnetic moments. In the future, these measurements should be extended towards more exotic isotopes to provide benchmarks for future developments of multi-reference DFT. Furthermore, measurements of the g-factors of the $I = 1/2^-$ states towards both neutron shell closures would help understand the discrepancy between DFT and experiment presented in this work.

Declaration of competing interest

The authors declare that they have no known competing financial interests or personal relationships that could have appeared to influence the work reported in this paper.

Data availability

Data will be made available on request.

Acknowledgements

This work was partially supported by the STFC Grant Nos. ST/M006433/1, ST/P003885/1, ST/V001035/1, ST/P004598/1 and ST/P004423/1, and by the Polish National Science Centre under Contract No. 2018/31/B/ST2/02220. RPDG received funding from the European Union's Horizon 2020 research and innovation programme under the Marie Skłodowska-Curie grant agreement No 844829. We acknowledge the CSC-IT Center for Science Ltd., Finland, for the allocation of computational resources. This project was partly undertaken on the Viking Cluster, which is a high performance compute facility provided by the University of York. We are grateful for computational support from the University of York High Performance Computing service, Viking and the Research Computing team. The funding from the European Union's Horizon 2020 research and innovation program under grant agreement No. 771036 (ERC CoG MAIDEN) and Academy of Finland (Grant Nos. 314733, 320062, 318043, 295207 and 327629) are gratefully acknowledged. We acknowledge W. Nörtershäuser for the use of the charge-exchange cell.

References

[1] W. Nazarewicz, Challenges in nuclear structure theory, J. Phys. G, Nucl. Part. Phys. 43 (2016) 044002.
[2] G. Neyens, M. Kowalska, D. Yordanov, K. Blaum, P. Himpe, P. Lievens, S. Mallion, R. Neugart, N. Vermeulen, Y. Utsuno, et al., Measurement of the spin and magnetic moment of Mg 31: evidence for a strongly deformed intruder ground state, Phys. Rev. Lett. 94 (2005) 022501.
[3] K. Flanagan, P. Vingerhoets, M. Avgoulea, J. Billowes, M. Bissell, K. Blaum, B. Cheal, M. De Rydt, V. Fedosseev, D. Forest, et al., Nuclear spins and magnetic moments of ^{71,73,75}Cu: inversion of $\pi 2p_{3/2}$ and $\pi 1f_{5/2}$ levels in ^{75}Cu, Phys. Rev. Lett. 103 (2009) 142501.
[4] J. Papuga, M. Bissell, K. Kreim, K. Blaum, B. Brown, M. De Rydt, R.G. Ruiz, H. Heylen, M. Kowalska, R. Neugart, et al., Spins and magnetic moments of ^{49}K and ^{51}K: establishing the $1/2^+$ and $3/2^+$ level ordering beyond N = 28, Phys. Rev. Lett. 110 (2013) 172503.
[5] R. Ferrer, N. Bree, T.E. Cocolios, I. Darby, H. De Witte, W. Dexters, J. Diriken, J. Elseviers, S. Franchoo, M. Huyse, et al., In-gas-cell laser ionization spectroscopy in the vicinity of 100Sn: magnetic moments and mean-square charge radii of N = 50–54Ag, Phys. Lett. B 728 (2014) 191–197.
[6] A. Klose, K. Minamisono, A.J. Miller, B. Brown, D. Garand, J. Holt, J. Lantis, Y. Liu, B. Maaß, W. Nörtershäuser, et al., Ground-state electromagnetic moments of ^{37}Ca, Phys. Rev. C 99 (2019) 061301.
[7] R. De Groote, J. Billowes, C. Binnersley, M. Bissell, T.E. Cocolios, T.D. Goodacre, G.J. Farooq-Smith, D. Fedorov, K. Flanagan, S. Franchoo, et al., Dipole and quadrupole moments of $^{73-78}$Cu as a test of the robustness of the Z = 28 shell closure near ^{78}Ni, Phys. Rev. C 96 (2017) 041302.
[8] D.T. Yordanov, L.V. Rodríguez, D.L. Balabanski, J. Bieroń, M.L. Bissell, K. Blaum, B. Cheal, J. Ekman, G. Gaigalas, R.F. Garcia Ruiz, et al., Structural trends in atomic nuclei from laser spectroscopy of tin, Commun. Phys. 3 (2020) 1–9.
[9] L. Rodríguez, D. Balabanski, M. Bissell, K. Blaum, B. Cheal, G. De Gregorio, J. Ekman, R.G. Ruiz, A. Gargano, G. Georgiev, et al., Doubly-magic character of ^{132}Sn studied via electromagnetic moments of ^{133}Sn, Phys. Rev. C 102 (2020) 051301.
[10] S. Pastore, S.C. Pieper, R. Schiavilla, R. Wiringa, Quantum Monte Carlo calculations of electromagnetic moments and transitions in A≤ 9 nuclei with meson-exchange currents derived from chiral effective field theory, Phys. Rev. C 87 (2013) 035503.
[11] M. Borrajo, J.L. Egido, Ground-state properties of even and odd magnesium isotopes in a symmetry-conserving approach, Phys. Lett. B 764 (2017) 328–334.
[12] J. Li, J. Meng, Nuclear magnetic moments in covariant density functional theory, Front. Phys. 13 (2018) 1–18.
[13] S. Péru, S. Hilaire, S. Goriely, M. Martini, Description of magnetic moments within the Gogny Hartree-Fock-Bogolyubov framework: application to Hg isotopes, Phys. Rev. C 104 (2021) 024328.
[14] P. Sassarini, J. Dobaczewski, J. Bonnard, R.G. Ruiz, Nuclear DFT analysis of electromagnetic moments in odd near doubly magic nuclei, J. Phys. G, Nucl. Part. Phys. 49 (2022) 11LT01.
[15] J. Bonnard, J. Dobaczewski, G. Danneaux, M. Kortelainen, Nuclear DFT electromagnetic moments in heavy deformed open-shell odd nuclei, Phys. Lett. B 843 (2023) 138014.
[16] A.R. Vernon, R.F. Garcia Ruiz, T. Miyagi, C.L. Binnersley, J. Billowes, M.L. Bissell, J. Bonnard, T.E. Cocolios, J. Dobaczewski, G.J. Farooq-Smith, K.T. Flanagan, G. Georgiev, W. Gins, R.P. de Groote, R. Heinke, J.D. Holt, J. Hustings, Á. Koszorús, D. Leimbach, K.M. Lynch, G. Neyens, S.R. Stroberg, S.G. Wilkins, X.F. Yang, D.T. Yordanov, Nuclear moments of indium isotopes reveal abrupt change at magic number 82, Nature 607 (2022) 260–265.
[17] M. Reponen, R.P. de Groote, L. Al Ayoubi, O. Beliuskina, M.L. Bissell, P. Campbell, L. Cañete, B. Cheal, K. Chrysalidis, C. Delafosse, A. de Roubin, C.S. Devlin, T. Eronen, R.F. Garcia Ruiz, S. Geldhof, W. Gins, M. Hukkanen, P. Imgram, A. Kankainen, M. Kortelainen, Á. Koszorús, S. Kujanpää, R. Mathieson, D.A. Nesterenko, I. Pohjalainen, M. Vilén, A. Zadvornaya, I.D. Moore, Evidence of a sudden increase in the nuclear size of proton-rich silver-96, Nat. Commun. 12 (2021) 4596.
[18] Z.Q. Chen, Z.H. Li, H. Hua, H. Watanabe, C.X. Yuan, S.Q. Zhang, G. Lorusso, S. Nishimura, H. Baba, F. Browne, et al., Proton shell evolution below ^{132}Sn: first measurement of low-lying β-emitting isomers in ^{123,125}Ag, Phys. Rev. Lett. 122 (2019) 212502.
[19] S. Eliseev, K. Blaum, M. Block, C. Droese, M. Goncharov, E. Minaya Ramirez, D.A. Nesterenko, Y.N. Novikov, L. Schweikhard, Phase-imaging ion-cyclotron-resonance measurements for short-lived nuclides, Phys. Rev. Lett. 110 (2013) 082501.
[20] P. Karvonen, I. Moore, T. Sonoda, T. Kessler, H. Penttilä, K. Peräjärvi, P. Ronkanen, J. Äystö, A sextupole ion beam guide to improve the efficiency and beam quality at IGISOL, Nucl. Instrum. Methods Phys. Res., Sect. B 266 (2008) 4794–4807.
[21] A. Nieminen, J. Huikari, A. Jokinen, J. Äystö, P. Campbell, E. Cochrane, Beam cooler for low-energy radioactive ions, Nucl. Instrum. Methods Phys. Res. A 469 (2001) 244–253.
[22] T. Eronen, et al., JYFLTRAP: a Penning trap for precision mass spectroscopy and isobaric purification, Eur. Phys. J. A 48 (2012) 46.
[23] L. Vormawah, M. Vilén, R. Beerwerth, P. Campbell, B. Cheal, A. Dicker, T. Eronen, S. Fritzsche, S. Geldhof, A. Jokinen, et al., Isotope shifts from collinear laser spectroscopy of doubly charged yttrium isotopes, Phys. Rev. A 97 (2018) 042504.
[24] R. de Groote, A. de Roubin, P. Campbell, B. Cheal, C. Devlin, T. Eronen, S. Geldhof, I. Moore, M. Reponen, S. Rinta-Antila, M. Schuh, Upgrades to the collinear laser spectroscopy experiment at the IGISOL, Nucl. Instrum. Methods Phys. Res., Sect. B, Beam Interact. Mater. Atoms 463 (2020) 437–440.
[25] S. Geldhof, M. Kortelainen, O. Beliuskina, P. Campbell, L. Caceres, L. Cañete, B. Cheal, K. Chrysalidis, C. Devlin, R. de Groote, et al., Impact of nuclear deformation and pairing on the charge radii of palladium isotopes, Phys. Rev. Lett. 128 (2022) 152501.
[26] M. Vilén, L. Canete, B. Cheal, A. Giatzoglou, R. de Groote, A. de Roubin, T. Eronen, S. Geldhof, A. Jokinen, A. Kankainen, et al., A new off-line ion source facility at IGISOL, Nucl. Instrum. Methods Phys. Res., Sect. B, Beam Interact. Mater. Atoms 463 (2020) 382–383.
[27] W. Gins, R.P. de Groote, M.L. Bissell, C.G. Buitrago, R. Ferrer, K.M. Lynch, G. Neyens, S. Sels, Analysis of counting data: development of the SATLAS python package, Comput. Phys. Commun. 222 (2018) 286–294.
[28] N. Stone, Table of nuclear electric quadrupole moments, At. Data Nucl. Data Tables 111 (2016) 1–28.
[29] T. Mertzimekis, K. Stamou, A. Psaltis, An online database of nuclear electromagnetic moments, Nucl. Instrum. Methods Phys. Res., Sect. A, Accel. Spectrom. Detect. Assoc. Equip. 807 (2016) 56–60.
[30] W. Sahm, A. Schwenk, Precision measurements of magnetic moments of nuclei with weak NMR signals, Z. Naturforsch. A 29 (1974) 1763–1766.
[31] P. Raghavan, Table of nuclear moments, At. Data Nucl. Data Tables 42 (1989) 189–291.
[32] H. Dahmen, S. Penselin, Measurement of the nuclear magnetic dipole moment of Au197 and hyperfine structure measurements in the ground states of Au197, Ag107, Ag109 and K39, Z. Phys. 200 (1967) 456–466.
[33] I. Berkes, B. Hlimi, G. Marest, E.H. Sayouty, R. Coussement, F. Hardeman, P. Put, G. Scheveneels, Static quadrupole moments of ^{106}Ag^m and ^{109}Ag^m and the electric field gradient of Ag in Zn and Cd, Phys. Rev. C 30 (1984) 2026–2030.
[34] W. Fischer, H. Hühnermann, T. Meier, Nuclear moments and optical isotope shifts of ^{108m}Ag and ^{110m}Ag, Z. Phys. A, At. Nucl. 274 (1975) 79–85.

[35] J. Carlsson, P. Jönsson, L. Sturesson, Accurate time-resolved laser spectroscopy on silver atoms, Z. Phys., D At. Mol. Clust. 16 (1990) 87–90.
[36] H. Bucka, D. Einfeld, J. Ney, J. Wilken, Untersuchung des $5p^2p_{3/2}$-Terms im Silber I-Spektrum durch Resonanzstreuung von Licht in elektrischen und magnetischen Feldern, Z. Naturforsch. A 26 (1971) 1016–1020.
[37] S. Eliseev, et al., A phase-imaging technique for cyclotron-frequency measurements, Appl. Phys. B 114 (2014) 107–128.
[38] D.A. Nesterenko, et al., Phase-Imaging Ion-Cyclotron-Resonance technique at the JYFLTRAP double Penning trap mass spectrometer, Eur. Phys. J. A 54 (2018) 154.
[39] G. Savard, S. Becker, G. Bollen, H.J. Kluge, R.B. Moore, T. Otto, L. Schweikhard, H. Stolzenberg, U. Wiess, A new cooling technique for heavy ions in a Penning trap, Phys. Lett. A 158 (1991) 247–252.
[40] M. Wang, W. Huang, F. Kondev, G. Audi, S. Naimi, The AME 2020 atomic mass evaluation (II). Tables, graphs and references, Chin. Phys. C 45 (2021) 030003.
[41] D. Nesterenko, T. Eronen, Z. Ge, A. Kankainen, M. Vilen, Study of radial motion phase advance during motion excitations in a Penning trap and accuracy of JYFLTRAP mass spectrometer, Eur. Phys. J. A 57 (2021) 302.
[42] C. Roux, et al., Data analysis of Q-value measurements for double-electron capture with SHIPTRAP, Eur. Phys. J. D 67 (2013) 146.
[43] R. Ringle, High-precision mass measurement of ^{38}Ca and development of the LEBIT 9.4-T Penning trap system, Ph.D. thesis, Michigan State University, 2006.
[44] F. Kondev, M. Wang, W. Huang, S. Naimi, G. Audi, The NUBASE2020 evaluation of nuclear physics properties, Chin. Phys. C 45 (2021) 030001.
[45] J. Blachot, Nuclear data sheets for A = 113, Nucl. Data Sheets 111 (2010) 1471–1618.
[46] B. Fogelberg, Y. Zongyuan, B. Ekström, E. Lund, K. Aleklett, L. Sihver, Isomerism, total decay energies, and absolute γ-ray intensities of the heavy Pd and Ag isotopes, Z. Phys. A, At. Nucl. 337 (1990) 251–255.
[47] N.D. Gamage, R. Sandler, F. Buchinger, J.A. Clark, D. Ray, R. Orford, W.S. Porter, M. Redshaw, G. Savard, K.S. Sharma, et al., Precise Q value measurements of ^{112,113}Ag and ^{115}Cd with the Canadian Penning trap for evaluation of potential ultra-low Q value β-decays, arXiv preprint, arXiv:2202.12874, 2022.
[48] J. Blachot, Nuclear data sheets for A = 115, Nucl. Data Sheets 113 (2012) 2391–2535.
[49] J. Kurpeta, A. Abramuk, T. Rząca-Urban, W. Urban, L. Canete, T. Eronen, S. Geldhof, M. Gierlik, J.P. Greene, A. Jokinen, A. Kankainen, I.D. Moore, D.A. Nesterenko, H. Penttilä, I. Pohjalainen, M. Reponen, S. Rinta-Antila, A. de Roubin, G.S. Simpson, A.G. Smith, M. Vilén, β- and γ-spectroscopy study of ^{119}Pd and ^{119}Ag, Phys. Rev. C 105 (2022) 034316.
[50] G.K. Woodgate, R.W. Hellwarth, Hyperfine structure of radioactive silver $^{111}_{47}$Ag, Proc. Phys. Soc. A 69 (1956) 581–587.
[51] Y.W. Chan, W.B. Ewbank, W.A. Nierenberg, H.A. Shugart, Nuclear spins and hyperfine-structure separations of silver-112 and silver-113, Phys. Rev. 133 (1964) B1138–B1144.
[52] U. Dinger, J. Eberz, G. Huber, R. Menges, R. Kirchner, O. Klepper, T. Ku, D. Marx, et al., Nuclear moments and change in the charge radii of neutron-deficient silver isotopes, Nucl. Phys. A 503 (1989) 331–348.
[53] J. Eberz, U. Dinger, G. Huber, H. Lochmann, R. Menges, R. Neugart, R. Kirchner, O. Klepper, T. Kühl, D. Marx, G. Ulm, K. Wendt, Spins, moments and mean square charge radii of $^{104--127}$In determined by laser spectroscopy, Nucl. Phys. A 464 (1987) 9–28.
[54] J. Dobaczewski, P. Bączyk, P. Becker, M. Bender, K. Bennaceur, J. Bonnard, Y. Gao, A. Idini, M. Konieczka, M. Kortelainen, L. Próchniak, A.M. Romero, W. Satuła, Y. Shi, L.F. Yu, T.R. Werner, Solution of universal nonrelativistic nuclear DFT equations in the Cartesian deformed harmonic-oscillator basis. (IX) HFODD (v3.06h): a new version of the program, J. Phys. G, Nucl. Part. Phys. 48 (2021) 102001.
[55] J. Dobaczewski, et al., 2023, to be published.
[56] J.A. Sheikh, J. Dobaczewski, P. Ring, L.M. Robledo, C. Yannouleas, Symmetry restoration in mean-field approaches, J. Phys. G, Nucl. Part. Phys. 48 (2021) 123001.
[57] M. Kortelainen, J. McDonnell, W. Nazarewicz, P.-G. Reinhard, J. Sarich, N. Schunck, M.V. Stoitsov, S.M. Wild, Nuclear energy density optimization: large deformations, Phys. Rev. C 85 (2012) 024304.
[58] Y. Shi, J. Dobaczewski, P.T. Greenlees, Rotational properties of nuclei around ^{254}No investigated using a spectroscopic-quality Skyrme energy density functional, Phys. Rev. C 89 (2014) 034309.
[59] M. Bender, J. Dobaczewski, J. Engel, W. Nazarewicz, Gamow-Teller strength and the spin-isospin coupling constants of the Skyrme energy functional, Phys. Rev. C 65 (2002) 054322.